Provenance and tectonic implications of Orán Group foreland basin sediments, Río Iruya canyon, NW Argentina (23° S)

William H. Amidon,* Lisa V. Luna,* George B. Fisher,† Douglas W. Burbank,†
Andrew R. C. Kylander-Clark† and Ricardo Alonso‡

*Middlebury College Geology Department, Middlebury, VT, USA
†Earth Research Institute, University of California, Santa Barbara, CA, USA
‡Departamento de Geología, Universidad Nacional de Salta, Salta, Argentina

ABSTRACT

Foreland basins are important recorders of tectonic and climatic processes in evolving mountain ranges. The Río Iruya canyon of NW Argentina (23° S) exposes *ca.* 7500 m of Orán Group foreland basin sediments, spanning over 8 Myr of near continuous deposition in the Central Andes. This study presents a record of sedimentary provenance for the Iruya Section in the context of a revised stratigraphic chronology. We use U–Pb zircon ages from six interbedded ash layers and new magnet-ostratigraphy to constrain depositional ages in the section between 1.94 and 6.49 Ma, giving an average sedimentation rate of $0.93 \pm 0.02\,(2\sigma)$ km Myr^{-1}. We then pair U–Pb detrital zircon dating with quartz trace-element analysis to track changes in sedimentary provenance from *ca.* 7.6 to 1.8 Ma. Results suggest that from *ca.* 7.6 to *ca.* 6.3 Ma, the Iruya watershed did not tap the Salta Group or Neogene volcanics that are currently exposed in the eastern Cordillera and Puna margin. One explanation is that a long-lived topographic barrier separated the eastern Puna from the foreland for much of the mid-late Miocene, and that the arrival of Jurassic-Neogene zircons records regional tectonic reactivation at *ca.* 6.3 Ma. A second major provenance shift at *ca.* 4 Ma is marked by changes in the zircon and quartz populations, which appear to be derived from a restricted source region in Proterozoic-Ordovician meta-sediments. Considered in conjunction with the onset of coarse conglomerate deposition, we attribute this shift to accelerated uplift of the Santa Victoria range, which currently defines the catchment's western limit. A third shift at *ca.* 2.3 Ma records an apparent disconnection of the Iruya with the eastern Puna, perhaps due to defeat of the proto Rio-Iruya by the rising Santa Victoria range. This study is one of the first applications of quartz trace-element provenance analysis, which we show to be an effective complement to U–Pb detrital zircon dating when appropriate statistical methods are applied.

INTRODUCTION

The eastern Central Andes (*ca.* 19–26° S) contain one of the world's best-exposed foreland basin sequences, which provides long-term records of climate and tectonics. The foreland record is a particularly useful archive of the signatures of recent tectonic events in the hinterland that are too young to be detected by thermochronology or defy direct structural observation (e.g. Deeken *et al.*, 2006; Ege *et al.*, 2007; and Carrapa *et al.*, 2012). Near continuous sedimentation has occurred in the eastern Andes since the Cretaceous, initially recording a rift environment, later transitioning into foreland and intermontane basin environments as the Andean orogeny got underway (Decelles *et al.*, 2011). In many cases, foreland sediments

have been caught up and deformed by the eastward advancing deformation front, which continues to record ongoing deformation in the Subandean Belt (Decelles & Horton, 2003). This remarkable sedimentary succession thus records nearly every stage of Andean evolution – a trove of information about Andean tectonic evolution that continues to yield new insights.

Andean foreland sequences have successfully addressed several key questions about tectonic evolution in other parts of the Andes: when did the deformation front arrive in different parts of the eastern Andes; what was the spatial pattern of rock uplift and erosion; and how was sediment routed through the growing ranges? (Hernández & Boll, 1986; Gubbels *et al.*, 1993; McQuarrie *et al.*, 2005, Strecker *et al.*, 2007; Uba *et al.*, 2009; Decelles *et al.*, 2011; Hain *et al.*, 2011; Del Papa *et al.*, 2013; Pingel *et al.*, 2013) Determining the provenance of distal foreland sediments is an efficient way to address these basic questions (e.g. Decelles *et al.*, 2011; Siks & Horton,

Correspondence: William H. Amidon, Geology Department, Middlebury College, Middlebury, VT 05753, USA. E-mail: wamidon@middlebury.edu

2011), because it integrates erosional signals from a large spatial area, while providing a nearly continuous record with *ca.* 100-kyr temporal precision. The gain or loss of unique provenance signatures can often be linked to specific watershed reorganization events driven by tectonic uplift or headward drainage capture (Amidon *et al.*, 2005a,b; Horton *et al.*, 2010). Such records are most effective under two conditions: the depositional ages of the foreland sediments must be robustly constrained, and geochemical provenance indicators must be traceable to distinct source areas. The Andes are an ideal place to apply such techniques because abundant volcanic tephra provide excellent age control, while a variety of lithologies and young volcanic rocks provide remarkably diagnostic sediment fingerprints.

In this article, we present a record of sediment provenance for the Orán Group in the Río Iruya section in NW Argentina, one of the longest and best exposed foreland sections in the Subandean zone (Fig. 1). The Rio Iruya section records the tectonic evolution of the east-central
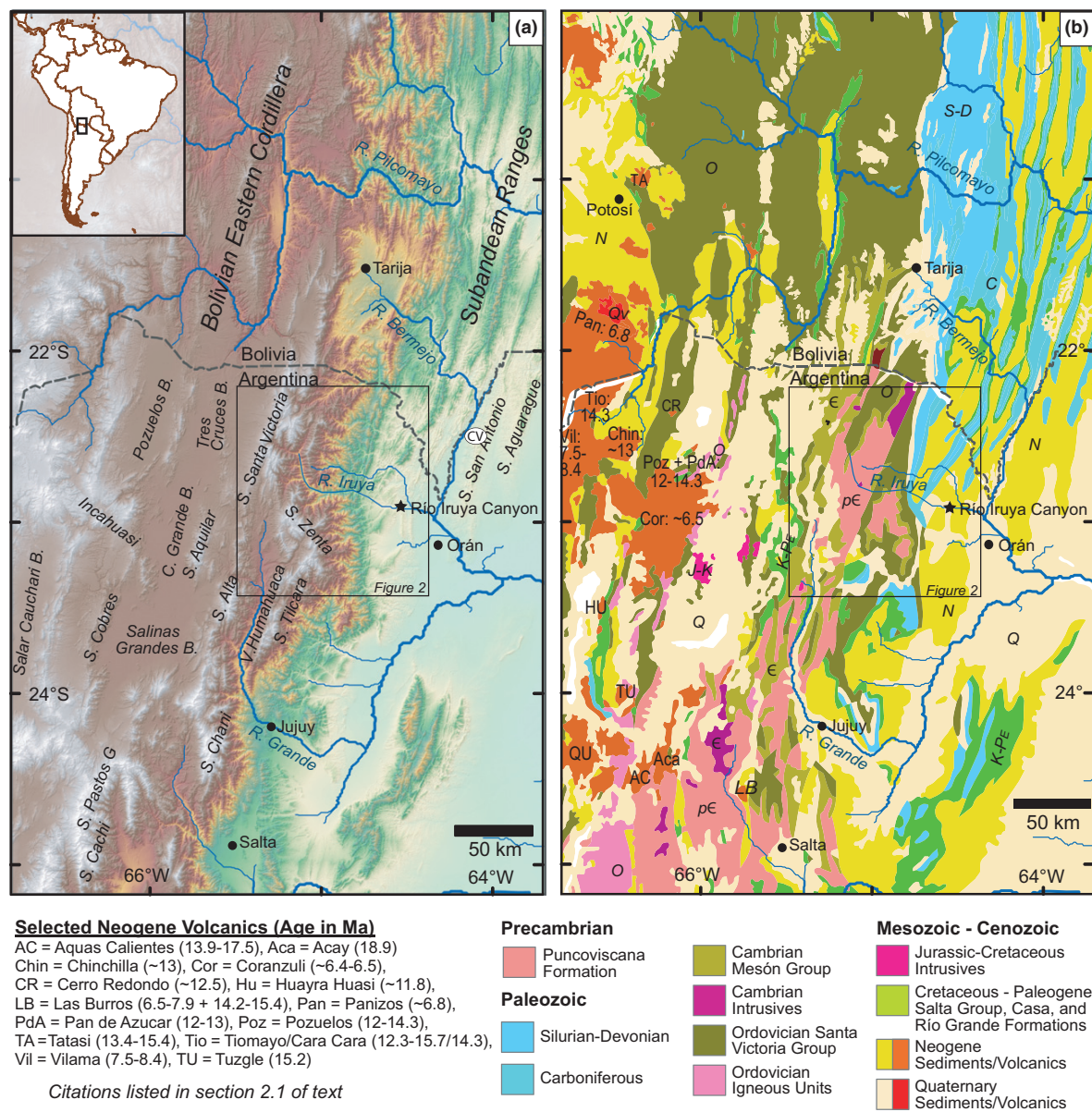

Selected Neogene Volcanics (Age in Ma)
AC = Aquas Calientes (13.9-17.5), Aca = Acay (18.9)
Chin = Chinchilla (~13), Cor = Coranzuli (~6.4-6.5),
CR = Cerro Redondo (~12.5), Hu = Huayra Huasi (~11.8),
LB = Las Burros (6.5-7.9 + 14.2-15.4), Pan = Panizos (~6.8),
PdA = Pan de Azucar (12-13), Poz = Pozuelos (12-14.3),
TA = Tatasi (13.4-15.4), Tio = Tiomayo/Cara Cara (12.3-15.7/14.3),
Vil = Vilama (7.5-8.4), TU = Tuzgle (15.2)

Citations listed in section 2.1 of text

Precambrian
- Puncoviscana Formation

Paleozoic
- Silurian-Devonian
- Carboniferous

- Cambrian Mesón Group
- Cambrian Intrusives
- Ordovician Santa Victoria Group
- Ordovician Igneous Units

Mesozoic - Cenozoic
- Jurassic-Cretaceous Intrusives
- Cretaceous - Paleogene Salta Group, Casa, and Río Grande Formations
- Neogene Sediments/Volcanics
- Quaternary Sediments/Volcanics

Fig. 1. (a) Topography of northwestern Argentina and southern Bolivia. Topography based on SRTM 90 m DEM and hydrology from HYDRO1K. CV denotes the location of Campamento Vespucio, where the Rio Seco formation was sampled (Decelles *et al.*, 2011) (b) Bedrock geology after 1 : 2 500 000 scale bedrock map of Argentina using data available from SEGEMAR and 1 : 1 000 000 scale bedrock map of Bolivia using data from GeoBolivia. Geologic naming conventions are Argentine and have been matched with corresponding Bolivian units. Labelling conventions: 'S' denotes Sierra, 'B' denotes basin, 'R' denotes river and 'V' denotes valley. Ages of volcanic centres are compiled from Salisbury *et al.* (2011), Kay & Coira (2009), Mazzuoli *et al.* (2008), Prezzi & Gõtze (2006), Caffe *et al.* (2002), Petrinovic *et al.* (1999), Cladouhos *et al.* (1994), Coira *et al.* (1993).

Andes near 22.5° S, which is less studied than areas immediately to the north and south. A human-induced diversion event caused the river to carve a new channel that has incised up to 100 m in about 100 years, creating spectacular exposures throughout the entire Mio-Pliocene section. To constrain the depositional ages of sediments in this section, we use U–Pb zircon geochronology and magnetostratigraphy to revise a previously published age model for the section (Hernández *et al.*, 1996). To track provenance changes over time, we combine detrital zircon U–Pb dating with trace-element compositions in quartz. Quartz geochemistry complements U–Pb zircon dating, because it reduces issues of both recycling and zircon fertility and is sensitive to a range of igneous and metamorphic conditions (Götze, 2009). We show that applying principal component analysis and clustering algorithms to quartz data can identify unique compositional populations of quartz and constrain the extent of the paleo-watershed. Our combined results identify three major shifts in sediment provenance that occur at *ca.* 6.7–6.0, *ca.* 4.3–3.5, and *ca.* 2.4–2.1 Ma, which we interpret as recording tectonic events within the Santa Victoria range and surrounding region.

OVERVIEW

Geologic setting

The Mio-Pliocene Río Iruya section is exposed in the eastern Andean foreland at a latitude of approximately 22.5° S. Bedrock exposed just west of this region consists primarily of Proterozoic to Mesozoic meta-sedimentary units deposited along the western margin of the South America Shield (Fig. 1). Extensive back-arc rifting during the Cretaceous deposited an overlying succession of clastic rocks, which is generally known as the Salta Group (Salfity & Marquillas, 1994; Viramonte *et al.*, 1999). The onset of the Andean orogeny changed depositional geometries by generating numerous mountain belts and intermontane basins, inverting some rift basins and simultaneously creating new foreland basins. The Salta Group thus grades upwards into Cenozoic foreland strata such as the Casa Grande, Río Grande and Río Seco Formations, typically disrupted by unconformities recording regional tectonism (Decelles *et al.*, 2011). The Andean Orogeny was also accompanied by generally eastward migrating silicic volcanism that deposited extensive ignimbrite sheets, mostly <25 Ma in age (Coira *et al.*, 1993; Allmendinger *et al.*, 1997). Collectively this shortening and volcanism thickened the internally drained Puna Plateau, whose eastern edge is defined by a basement-cored compressional mountain range known as the Eastern Cordillera (or Cordillera Oriental). In our study area, the Eastern Cordillera is represented by the Santa Victoria range, which creates 4000 m of relief along the eastern escarpment of the Andes. East of this escarpment rise the smaller ranges of the Subandean Belt, a thin-skinned fold-and-thrust belt propagating eastward into foreland sediments. Our study focuses on the Oran Group, a package of interbedded conglomerates, sandstones and siltstones that are widely exposed in the northern Argentina foreland. The Iruya exposure sits near the southern termination of the Subandean Belt, where the structural style begins to transition southward into thick-skinned thrusting in the Santa Barbara System (Strecker *et al.*, 2007).

To the north (*ca.* 19–21°), construction of the Eastern Cordillera appears to have begun as early as 25 Ma and was largely completed by 8–12 Ma (Gubbels *et al.*, 1993; Kley *et al.*, 1997; Müller *et al.*, 2002; Elger *et al.*, 2005). The earliest deformation in the Bolivian Subandes is around 12.4 Ma and increased in intensity around 6 Ma (Uba *et al.*, 2009). To the south (*ca.* 24–26°), deformation in the Eastern Cordillera began around the same time, but appears to have continued into Pliocene time. Deformation progressed roughly west to east, with deformation in the Cumbres de Luracatao (*ca.* 66.5° W) range beginning around 21 Ma (Deeken *et al.*, 2006), reaching the Angastaco region (*ca.* 66° W) by *ca.* 14 Ma (Coutand *et al.*, 2006; Carrapa *et al.*, 2012). Further east, early phases of growth in the Santa Barbara System (the Subandean equivalent) are recorded in the Metán range (*ca.* 65.3° W) at *ca.* 10 Ma (Hain *et al.*, 2011). Deformation appears to have extended into the eastern Santa Barbara System (east of 65.3° W) very recently, mostly after 2 Ma (Hain *et al.*, 2011). Despite this generally eastward progression, there is also abundant evidence for diachronous uplift. For example, significant relief seems to have developed within the Eastern Cordillera after 5 Ma, as recorded by the development of intermontane basins (Carrera & Muñoz, 2008).

In our own study area near 23° S, uplift of ranges along the eastern Puna margin was underway by the middle Eocene to Oligocene (Hongn *et al.*, 2007; Insel *et al.*, 2012), and significant relief existed along the eastern margin to create deep basins and orographic barriers by *ca.* 10–8 Ma (Kleinert & Strecker, 2001; Starck *et al.*, 2001; Mulch *et al.*, 2010). Most studies suggest deformation in the Eastern Cordillera began during the middle Miocene. Facies migration of the Salta and Orán Groups places the onset of thrusting in the Eastern Cordillera at roughly 15 Ma (Decelles *et al.*, 2011). This timing is broadly consistent with the onset of deposition of the Orán Group between *ca.* 13.5–8 Ma (closer to 8 Ma in most places), which records the arrival of a foreland sedimentary wedge of poorly understood provenance (Hernández *et al.*, 1996; Reynolds *et al.*, 2000, 2001; Echavarria *et al.*, 2003). Two recent studies have illuminated the timing of localized deformation *ca.* 50–100 km to the southwest of the Río Iruya. Evidence from the Cianzo Basin (Fig. 2) suggests thrusting in the Eastern Cordillera began between 14 and 10 Ma based on the appearance of Salta Group clasts within the Río Grande and Pisungo Formations (Siks & Horton, 2011). However, generation of significant relief may not have occurred until the Late Miocene. For example, in the

nearby Humahuaca Valley renewed tectonism may be recorded by deposition of the Maimará formation at *ca.* 6.5 Ma, which then evolved into an isolated inter-montane basin by *ca.* 4.1 Ma (Pingel *et al.*, 2013). This timing is supported by stratigraphy from the Casa Grande Basin just to the west, which records uplift of the Sierra Alta around 4.3 Ma (Streit *et al.*, 2015).

Farther east, deformation in the Subandean Belt near *ca.* 22° S is interpreted to have begun as early as 8.5–9 Ma, followed by the eastward progression of in-se-quence thrusting (Echavarria *et al.*, 2003). Thrusts faults splay from a detachment within Silurian shales causing folding in the overlying Silurian to Tertiary sediments and creation of the Subandean ranges in the hanging walls above the Cinco Picachos, Pescado, and Pintascayo thrusts (Fig. 2). Movement on the Cinco Picachos back thrust is interpreted to have begun between 9 and 8.5 Ma based on an observed acceleration in sedimentation rates in Orán Group sediments (Echavarria *et al.*, 2003). The

Pintascayo thrust is interpreted to have been active between *ca.* 7.6 Ma and 5 Ma, after which deformation continued eastward to the San Antonio Range (*ca.* 4.5–4 Ma), and Aguarague range (*ca.* 3–1.2 Ma) (Fig. 1) (Echavarria *et al.*, 2003). The Subandean ranges may also have experienced subsequent out-of-sequence thrusting. A provenance change at *ca.* 4.5 Ma in the Río Iruya section has been attributed to out-of-sequence reactiva-tion of the Pescado fault (Fig. 2) (Hernández *et al.*, 1996). Reactivation may have continued into the Quater-nary as suggested by sequence-capping gravels of the El Simbolar Formation. These strata are interpreted to have been deposited in range-bounded intermontane basins due to reactivation of the El Pescado and Pintascayo thrusts after ca. 2.3 Ma (Echavarria *et al.*, 2003).

The Río Iruya canyon exposes *ca.* 7.5 km of foreland basin sediments, which are part of the regionally mapped Orán Group (Russo, 1975). The age of the section is previously interpreted to range from *ca.* 13.5 to 0.8 Ma
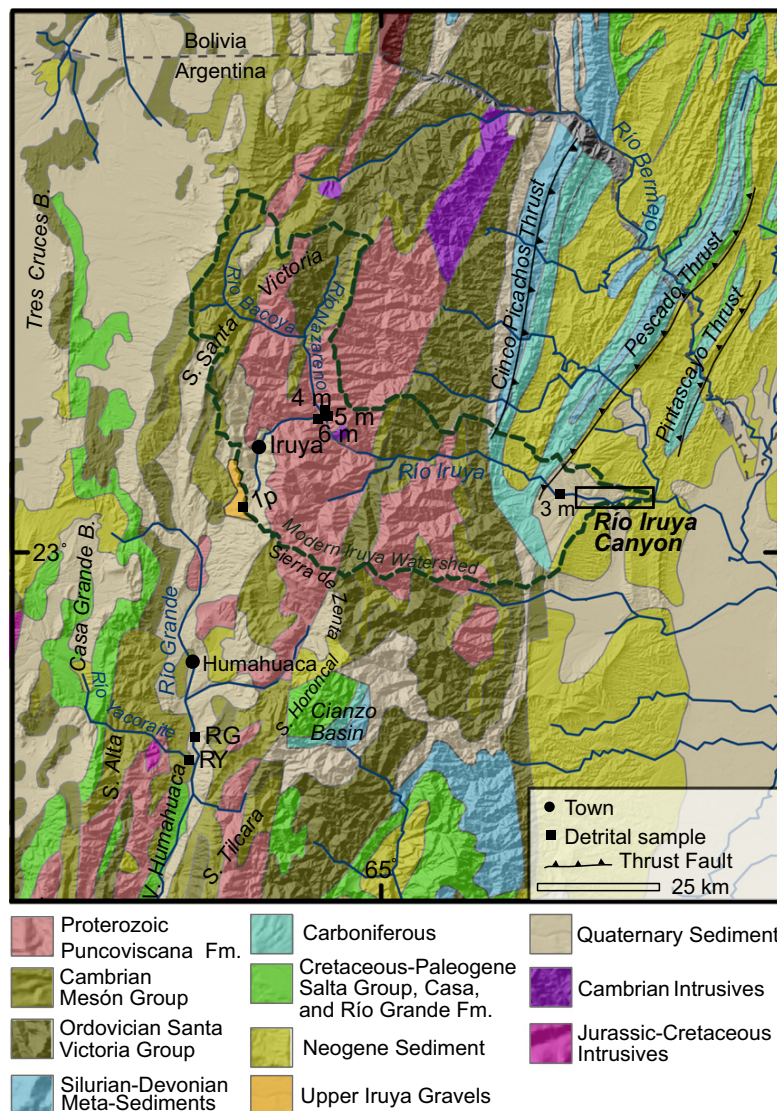

Fig. 2. Detailed map of study area including the Río Iruya Canyon, nearby Subandean thrusts, and detrital sampling locations: 3 m = Rio Iruya; 4 m = Rio Nazareno; 5 m = 'Puncovscana fan'; 6 m = Upper Rio Iruya; 1p = Upper Iruya Gravels. RG and RY denote the Rio Grande and Rio Yacoraite samples from Streit *et al.* (2015). Topography from SRTM 90 m DEM.

Fig. 3. Stratigraphic column and magnetostratigraphy for the Río Iruya section. Stratigraphic thicknesses were measured in the field or calculated using GPS locations, ASTER GDEM elevations, and strikes and dips taken in the field. Generalized stratigraphy is after Hernández *et al.* (1996). Interbedded ash ages represent the preferred eruption age (see Fig. 5 for details). VGP latitudes were determined as described in section 4.2. Detrital zircon sample ages were calculated based on the stratigraphic age model described in section 4.3 and are estimated to have errors of <100 000 years. The magnetic polarity timescale (MPS) summarizes our own data in block form, whereas the global polarity time scale (GPTS) is from the global compilation of Lourens *et al.* (2004).
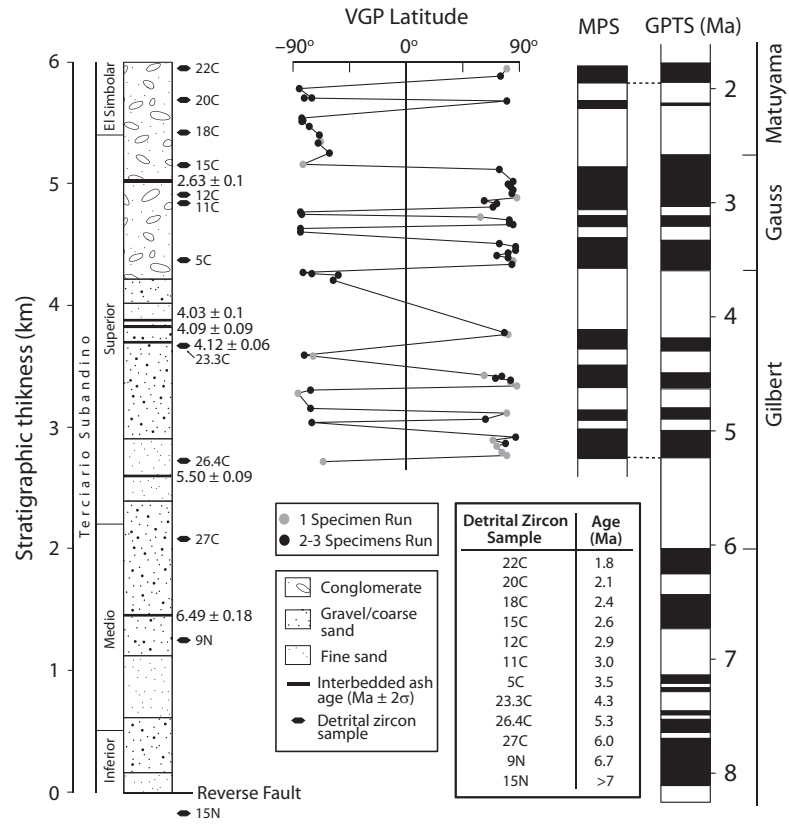
based on magnetostratigraphy and tephrachronology (Hernández *et al.*, 1996, 1999). Based on the previous interpretation, sedimentation rates average *ca.* 1.01 mm per year from *ca.* 9.5 to 3.0 Ma, then decline to *ca.* 0.42 mm per year after 3.0 Ma (Echavarria *et al.*, 2003; Hernández & Echavarria, 2009). The Orán Group is typically broken into three stratigraphic units: the Tranquitas, the Terciario Subandino, and the El Simbolar formations (Russo, 1975; Hernández *et al.*, 1996). The Terciario Subandino constitutes the majority of the section and is further subdivided into three prograding sequences: the Inferior, Medio and Superior (Fig. 3). Paleocurrent indicators suggest that all units were deposited from west or northwest (Hernández *et al.*, 1996). *The Inferior* is interpreted to have been deposited in a distal foreland basin, whereas the *Medio, Superior* and El Simbolar are thought to be coeval with Subandean structural growth (Hernández *et al.*, 1996).

METHODS

Magnetostratigraphy

The motivation to replicate magnetostratigraphy along a previously dated section is that rapid vertical and lateral erosion rates (metres per year) prevent precise relocation of the existing paleomagnetic sites. Nonetheless, our revised chronology is linked to the previous one through a set of annotated air photos provided by Dr James

Reynolds, which were used to visually relocate existing paleomagnetic sites (Fig. 4). Although changes in the shape of the canyon between the 1980s and 2012 caused significant error in this relocation, we estimate the precision to be within ±20 m stratigraphically of their original location. Our section begins at 22.90345° S and 64.52103° W and ends at 22.896012° S, 64.645613° W (WGS 84).

Magnetostratigraphy samples in mudstones and siltstones were collected through *ca.* 3000 m of continuously exposed stratigraphic section. One hundred and four block samples were excavated at a spacing of *ca.* 30 m, drilled and cut using air and nonmagnetic bits and blades, and then measured at the Caltech Paleomagnetics Laboratory. Remanent magnetizations for all samples were measured using a 2G Enterprises DC SQuID three-axis cryogenic magnetometer housed in a magnetically shielded room and equipped with computer-controlled alternating field (AF) demagnetization coils and automated sample changer system (Kirschvink *et al.*, 2008). Background noise for the magnetometer is <1 pAm^2, and all thermal demagnetization steps were performed in a nitrogen atmosphere within a magnetically shielded ASC™ oven.

Of the 104 collected sites, 21 were destroyed during transport and/or preparation. An attempt was made to run two specimens from each site, preferably from separate cores when possible, yielding a total of 155 specimens from 83 sites. These 155 specimens were first analysed for natural remanent magnetization (NRM) and then cooled
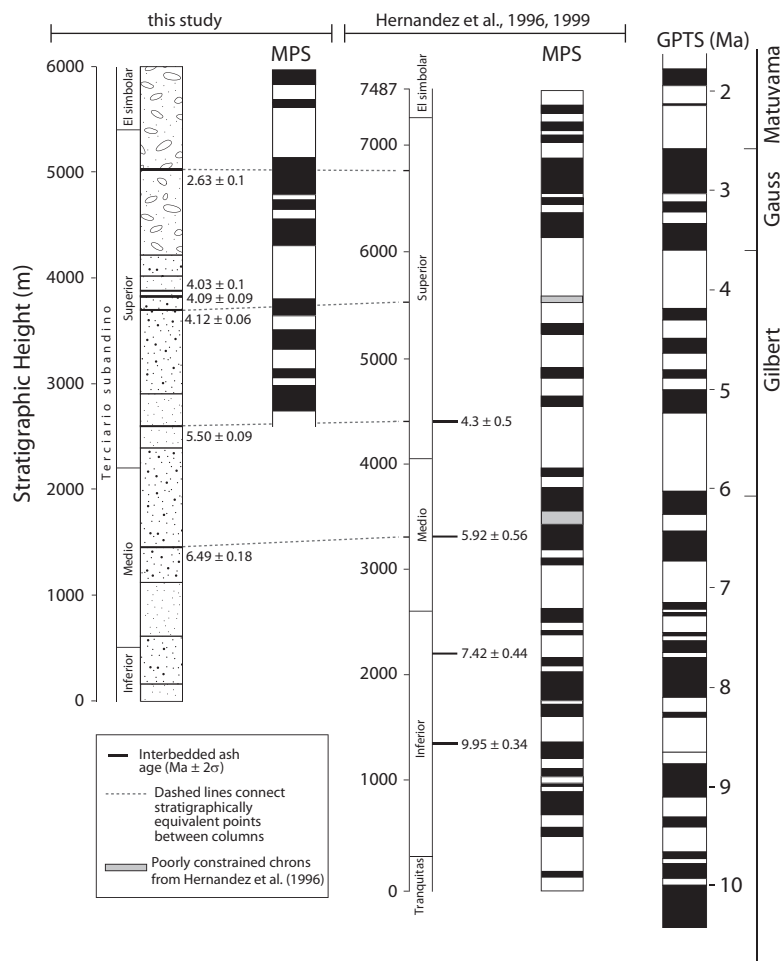
Fig. 4. Comparison of magnetostratigraphy and interbedded ash ages from this study with magnetostratigraphy and ash ages published in Hernández *et al.* (1996) and updated in Hernández *et al.* (1999). Specific tie points between the two columns were correlated using annotated aerial imagery of previously sampled sites (J. Reynolds, pers. comm.). Stratigraphic thicknesses generally match well between the columns, and small discrepancies in stratigraphic thickness likely reflect inherent errors in measuring section. The top of the section is revised to be *ca.* 0.6 Myr older than previously thought.

twice in a liquid nitrogen (LN$_2$) bath for >20 min to remove potential multi–domain viscous magnetizations. The specimens were then subjected to AF demagnetizations in 2.5 mT steps from 2.5 to 7.5 mT to remove low-coercivity magnetizations. Lastly, stepwise thermal demagnetization was performed on the specimens in 50°C steps from 100°C to 500°C and then in 20–30°C steps up to *ca.* 680°C.

Stratigraphic section was measured over two intervals of 700 and 1300 m. To connect the measured sections and assign stratigraphic heights to tephra and detrital zircon samples within unmeasured section, unmeasured stratigraphic heights were calculated from GPS locations, ASTER GDEM elevations, and strikes and dips measured in the field.

U-Pb dating

U-Pb dating was applied to tephra for the purpose of age control and to detrital samples for provenance analysis. Zircons were separated from six interbedded tephra layers, mounted in epoxy, and polished parallel to the c-axis for analysis by laser ablation – inductively coupled plasma mass spectrometry (LA-ICPMS). Zircon analyses were performed at the UCSB LASS facility using a Photon Machines Analyte 193 nm excimer laser and Nu Instruments Plasma MC-ICPMS, following the methods described in Kylander-Clark *et al.* (2013). Analyses targeted the rims of zircons free of cracks or inclusions using a spot size of 30 μm and a rep rate of 4 Hz. Results were standardized using the 91 500 zircon reference material (Wiedenbeck, 1995). GJ1 (601.7 ± 1.3 Ma; Jackson *et al.*, 2004; D. Condon, pers. comm.) was used for quality control for ashes 1, 4 and 5. This standard yielded a mean $^{206}Pb/^{238}U$ age of 583.4 ± 7.8 ($n = 25$; MSWD = 1.9). Plesovice (337.13 ± 0.37 Ma: Sláma *et al.*, 2008) was used for quality control for ashes 6, 7, 8, yielding a mean $^{206}Pb/^{238}U$ age of 335.6 ± 2.4 Ma ($n = 6$; MSWD = 0.9).

Twelve detrital zircon samples were taken from the Orán Group with depositional ages ranging from *ca.* 10 Ma to 1.8 Ma. Two samples were taken from modern rivers: one from the Río Iruya just upstream of the section; and one from the Río Nazareno in the headwaters (Fig. 2; samples 4 m and 6 m). Two additional samples were analysed by Streit *et al.* (2015), one from the Rio Grande and another from the Rio Yacoraite, both just above their confluence (Fig. 2; samples RG and RY).

An additional estimated Mio–Pliocene-aged sample was taken from a gravel deposit exposed at the drainage divide between the upper Iruya and the Humahuaca basin, which we refer to as the 'upper Iruya gravel' sample (Fig. 2; sample 1p). These gravel deposits cap much of the ridgeline to the southwest of Iruya village, extending gently downslope to the west in the upper Rio Grande watershed (Fig. 2). Although the age of these deposits is unknown, their complete topographic inversion (e.g. their location on ridgelines), and their significant deflation suggests they are not associated with upper Pleistocene-aged fill. Paleocurrents are generally east-directed suggesting the deposits were once linked to the Mio-Pliocene Iruya foreland prior to disconnection by tectonic uplift.

For detrital zircons, fracture and inclusion-free zircon cores were targeted using a spot size of 15 μm and were ablated at a rate of 4 Hz. Given the increasing possibility of Pb loss with age, $^{238}U/^{206}Pb$ ages are used for <1200 Ma grains, and $^{207}Pb/^{206}Pb$ ages are used for >1200 Ma. Grains that showed >30% differences between $^{238}U/^{206}Pb$ and $^{235}U/^{207}Pb$ ages were rejected, except for grains <100 Ma, which were all utilized. To capture all significant age peaks in a given sample, 130–220 zircons were analysed in each sample. Detrital zircon results are displayed using probability density plots (PDFs) using a constant 1.5% analytical error to standardize visualization and comparison. Kolmorogov–Smirnov (K-S) tests were performed between pairs of samples to test the null hypothesis that they were drawn from the same zircon population (Table S3). The K–S test produces a *P*-value, which indicates the likelihood that the samples were drawn from different populations. For example, a *P*-value of 0.05 indicates 95% confidence that samples were drawn from different populations. K–S tests and PDFs were generated using software from the University of Arizona LaserChron center.

Quartz trace-element composition

Although trace-element variations in quartz have long been recognized, they have rarely been used as a provenance tool (e.g. Monecke *et al.*, 2002). Recent improvements in LA-ICPMS techniques make measurement of trace elements in quartz routine, opening the door to a range of provenance applications (Götze, 2009; Muller & Koch-Mueller, 2009). Quartz contains low concentrations of select trace elements such as Al, Cl, Na, K, Ca, Ti, Fe, P, B, Li and Ge (listed in generally descending order). Average concentrations in quartz range from *ca.* 500 ppm for Al down to *ca.* 1 ppm for Ge and span an order of magnitude for a given element. Elements such as Al^{+3}, Ti^{+4} and Fe^{+3}, are incorporated by direct substitution for Si^{+4}, whereas other cations, such as Li^+, Na^+ and K^+, can be incorporated in interstitial locations to balance charge (Götze, 2009). The petrologic controls on trace-element incorporation in quartz remain poorly understood, but always depend on the activity of multiple species in a fluid or melt. In igneous rocks, concentrations

of Ti and Al always increase with temperature, whereas concentrations of less compatible elements depend on the degree of magmatic differentiation and the stage of crystallization, e.g. enriched in late-stage pegmatites (Wark & Watson, 2006; Breiter *et al.*, 2013). It has recently been shown that quartz from different granitic types (A, S and I) can be distinguished based on the relative proportions of Al and Ti (Ackerson *et al.*, 2015). In metamorphic rocks, diffusive loss during metamorphism generally lowers the concentration of all trace elements, creating a potentially diagnostic provenance fingerprint (Götze, 2009; Muller & Koch-Mueller, 2009). Recent work has also focused on using cathodoluminescence textures of quartz as a provenance tool, although it is not clear how the preservation of these textures during metamorphism compares with the diffusive loss of trace elements from quartz (Augustsson *et al.*, 2011).

Within the Orán group, quartz was analysed from 11 of the same samples as detrital zircons. Additionally, four modern detrital samples were analysed from the upper Iruya (6 m), an alluvial fan sourcing the Puncoviscana Formation (5 m), the lower Río Iruya (3 m), and the Río Grande in the Quebrada de Humhuaca (RG) (Fig. 2). All analyses were performed on 300–1000 μm quartz grains mounted in epoxy and polished using SiC polishing grit. The elements Li, Be, B, Na, Mg, Al, P, Cl, K, Ca, Ti, Fe, Co, Ga, Ge, Y and Zr were measured by LA-ICPMS at Rensselaer Polytechnic Institute using a Photon Machines Analyte 193 nm excimer laser and a Bruker 820-MS ICPMS. Thirty to sixty individual quartz grains per sample were ablated at 6 Hz using an 80-μm square spot. Analyses were standardized using the NIST612 glass standard (Woodhead *et al.*, 2007), and an in-house synthetic quartz standard, prepared to 495 ± 70 ppm Al and 117 ± 24 ppm Ti, was used for quality assurance (N. Tailby, pers. comm.).

We have explored a variety of statistical methods to identify provenance signatures in the quartz data, which are discussed at length in a supplementary text document (Data S1).

RESULTS AND INTERPRETATION

U-Pb ages of volcanic tephra

Tephra ages range from 2.63 to 6.49 Ma (Fig. 5 and Table S1). All tephra ages are based on $^{206}Pb/^{238}U$ ages corrected for initial Pb and secular disequilibrium. Most analyses are slightly discordant, which we attribute to minor amounts of common Pb. We correct for this by assuming concordance, calculating a 207-corrected $^{206}Pb/^{238}U$ age using Isoplot (Ludwig, 1998), and assuming a common $^{207}Pb/^{206}Pb$ ratio of 0.84 (Stacey & Kramers, 1975). The magnitude of this age correction varies by sample, with sample Ash-7 showing the largest magnitude correction (*ca.* 10%) and most other samples resulting in ≤1% corrections. A second correction accounts for the exclusion of ^{230}Th during crystallization, causing a

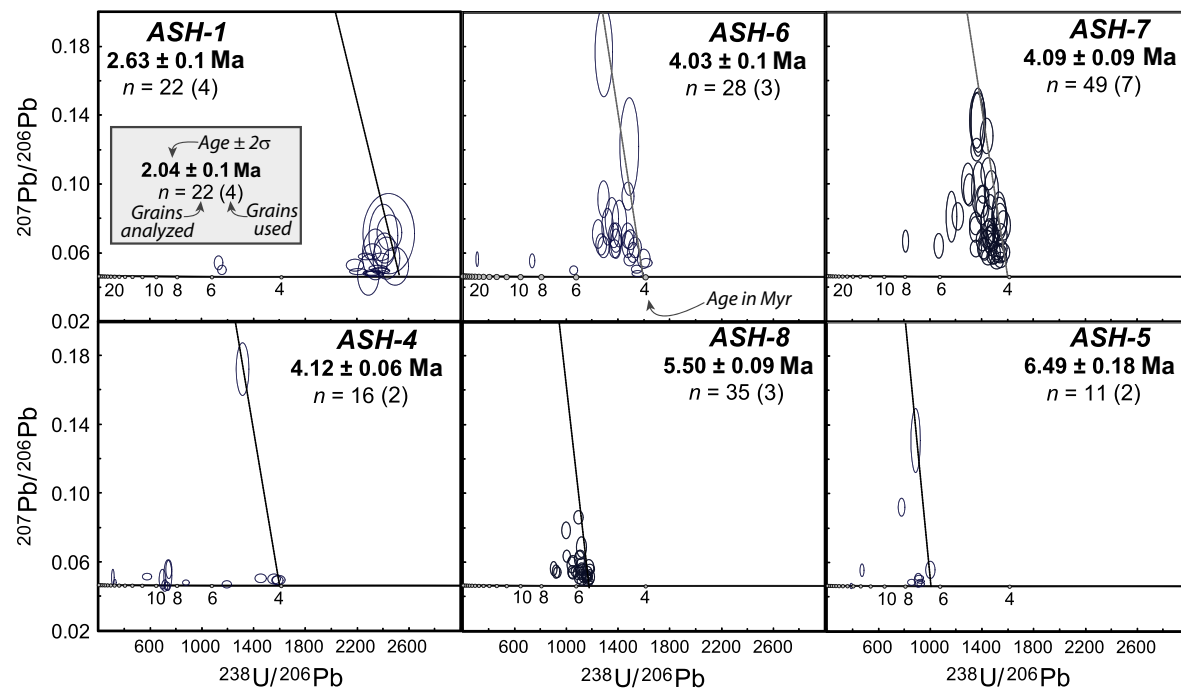**Fig. 5.** Tera–Wasserburg concordia plots of LA–ICPMS U–Pb zircon data for the six tephra samples displayed as 2σ error ellipses. Thin line represents the best-fit mixing line between an initial $^{207}Pb/^{206}Pb$ of 0.84 and the measured ratios of the youngest grains. Thick horizontal line is the concordia line with ages labelled in Ma. Preferred eruption ages are shown in bold, along with the # of grains dated (*n*) and the number used to estimate the preferred age (parentheses).

period of disequilibrium in the $^{238}U-^{206}Pb$ decay series and a resultant age underestimate. This correction follows Schaerer (1984) as described in Schoene (2013) and assumes a Th/U ratio of 3.2 based on an average value of Mio–Pliocene ignimbrites just west of the study area (Salisbury *et al.*, 2011).

Each of the six tephra beds yielded a distribution of U–Pb zircon ages reflecting differing degrees of contamination by zircons derived from pre-eruption country rock and reworking (Table S1). We assign eruptive ages based on the weighted mean age of the youngest cluster of zircons that overlap each other within 1σ uncertainty. This approach is justified by the fact that young zircons are unlikely to have experienced significant Pb loss that would lead to anomalously young ages, yet are virtually certain to have begun crystallizing hundreds of thousands of years prior to eruption (Brown & Fletcher, 1999).

Paleomagnetic results

The magnetic polarity stratigraphy records nine normal and nine reversed magnetozones that span a time period from *ca.* 1.8 to 5.2 Ma and include the entire Gauss chron and parts of the Matuyama and Gilbert chrons (Fig. S1). In all but one case, the polarity reversal boundaries were well delimited within the section based on only the magnetic polarity stratigraphy, such that tephras simply served as a general check. In the case of the polarity reversal marking the end of the Cochiti subchron at

ca. 4.187 Ma (Lourens *et al.*, 2004) – a boundary that is poorly defined by our magnetic data, we used the stratigraphic height of Ash-7 (4.09 ± 0.09 Ma) to delineate this transition into the long overlying reversal. Overall magnetostratigraphy in the Río Iruya canyon appears to capture all of the major chrons and subchrons of this segment of the global polarity timescale (Lourens *et al.*, 2004), thereby yielding a robust age model (Fig. 3).

Results from the stepwise thermal demagnetization of the Río Iruya specimens indicate a relatively consistent pattern whereby the majority of samples progress towards the origin until *ca.* 600°C, with this singular component interpreted to represent the characteristic remanent magnetization (ChRM) at the time of deposition (Fig. S1). Above *ca.* 600°C, specimen behaviour becomes erratic and is indicative of complete unblocking. This finding strongly suggests magnetite as the dominant magnetic carrier in our samples and is in agreement with earlier paleomagnetic work performed along the same section of the Río Iruya (J. Reynolds, pers. comm.). The lack of a significantly different low-temperature component and the negligible drop in magnetic intensity following liquid nitrogen treatments appear to indicate a general lack of viscous overprints or of any appreciable remanence related to multi-domain minerals.

ChRM directions for each specimen were determined using PaleoMag 3.1.0 b2 software (Jones, 2002). For each specimen between 4 and 12 points (including the origin) were used to delimit magnetic vectors using principle

component analysis (Kirschvink, 1980) implemented within the software. We note that in all cases the origin was used to help constrain ChRM direction because the demagnetization paths chosen always headed towards the origin. Of the 155 specimens analysed, 36 (*ca.* 23%) were discarded due to incoherent orthogonal demagnetization diagrams or maximum angular deviations (MAD) of >15°, yielding 68 sites and 119 specimens (average MAD of 6°). Overwhelmingly, samples that displayed incoherent demagnetization diagrams and high MADs were found at polarity boundaries and likely recorded unstable periods in Earth's magnetic field. Virtual geomagnetic poles (VGPs) were calculated from the resulting tilt-corrected specimens and their latitudes used to delineate periods of normal and reversed polarity (Fig. 3). Due to the homoclinal structure of the Río Iruya section, a fold test was not performed (Tauxe & Watson, 1994). However, the robust antipodal behaviour and tight clustering of the reversed and normal polarity samples following tilt-correction argues for a well-behaved system (Fig. S1).

Age model and sediment-accumulation rates

Our age model for the Río Iruya section spans 1.94–6.49 Ma (Fig. 4). Reversal boundary ages are assumed to lie at the stratigraphic mid-point between the adjacent samples of opposite polarity that define each reversal. Overall, the age-model fit is quite robust with 95th-percentile age confidence intervals of ±103 000 years on the boundary ages and with an average sedimentation rate of 0.93 ± 0.02 (2σ) km My^{-1} (Fig. 6). To observe contrasts in sedimentation rates through time, optimized, maximum (using the observed samples of opposite polarity bracketing the subchron) and minimum (using the observed samples of similar polarity bracketing the subchron) sediment-accumulation-rate curves were calculated using the age-thickness relationship for the magnetostratigraphy and Ash-5 (6.49 Ma) and Ash-8 (5.5 Ma). Other tephra were not used in the sediment-accumulation-rate calculations, because they tended to truncate short periods of time where small variations in thickness or age created excessive rates of deposition. This 'small interval effect' is also evident for the Reunion subchron (2.128–2.148 Ma) which is defined by one data point: this isolated normally magnetized site permits an infinitely high maximum accumulation rate and predicts suspiciously high rates (>4 km My^{-1}) even when using the mean boundaries between adjacent points. To remove these perceived artifacts in the dataset, we chose to fix the Reunion thickness at 18 m in the optimized calculation to approximately match the average overall sediment-accumulation rate for the section of *ca.* 1 km My^{-1}. Maximum and minimum accumulation rates were not calculated for the section between Ash-5 and Ash-8 due to the lack of constraints on the stratigraphic error.

From 5.5 to 1.8 Ma, sediment-accumulation rates are rapid and fall consistently between 0.7–1.3 km My^{-1} (Fig. 6). Whereas periods of pulsed increases in accumu-
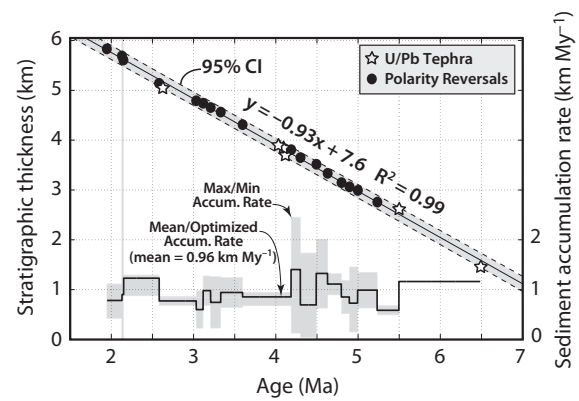
Fig. 6. Age vs stratigraphic height or sediment accumulation rate for all polarity changes and ash ages in the stratigraphic section (Fig. 3). Polarity changes were calculated as the middle point between adjacent points of opposite polarity. The maximum and minimum sediment-accumulation rates (grey bounds) were calculated by expanding and dilating the polarity bounds to the greatest extent, i.e. the observed samples of opposite polarity bracketing the subchron, and least extent, i.e. the observed samples of similar polarity bracketing the subchron, possible for each subchron.

lation rates (*ca.* 4.25–4.75 Ma and 2.15–2.5 Ma) do appear in our chronology, rates are, in general, steady (*ca.* 0.93 km My^{-1}) at the million-year timescale. This overall rate is in basic agreement with a previous estimate of *ca.* 0.77 km My^{-1} along this same section and time-span using a coarser sampling strategy and less precise measurements and ash ages. However, we see no decrease in sedimentation rates after 3 Ma, as previously observed (Hernández *et al.*, 1996).

To estimate an age for sample 9n for which we have no magnetostratigraphic control, we extrapolate the mean accumulation rate of the overlying section, as defined by the two U-Pb dates on ashes at 5.5 and 6.5 Ma, giving an age of 6.7 Ma (Fig. 3). The lowest sample (15n) is estimated to be *ca.* 7.6 Ma based on the original magnetostratigraphy and zircon fission-track dating of Hernández *et al.* (1996).

Detrital zircons in bedrock and modern rivers

Using detrital zircons to infer provenance is often ambiguous due to overlapping U-Pb age populations between source lithologies. Nonetheless, certain signature age peaks in the data can often be linked to specific source regions. Here use compiled detrital zircon age spectra from the published literature to identify three U-Pb age signatures that appear to be reliable proxies for specific source lithologies (Mcbride, 2008; Adams *et al.*, 2011; Decelles *et al.*, 2011; Siks & Horton, 2011).

First, the Pan-African signal is sometimes characterized by a 'double hump' pattern with a very large Pampean peak at *ca.* 520 Ma and a smaller peak near 640 Ma. The double hump is typical of Proterozoic-early

Paleozoic source rocks such as the Puncoviscana, Meson and Santa Victoria Group (Fig. 7), and is also observed in spectra from rivers that drain them, such as the Rio Nazareno (sample 4 m in Figs 2 and 8). In contrast, the Pan-African signal tends to appear as a single broad peak in younger source rocks.

A second signature is the presence or absence of Jurassic-Neogene zircons (*ca.* 25–200 Ma. These are not present in Paleozoic or older rocks, and tend to reliably occur in Jurassic- Eocene units such as the Tacuru

Group, Pirgua Subgroup, Santa Barbara Subgroup and Casa Grande Formation. Several small Jurassic plutons also dot the eastern Puna, such as the *ca.* 160 Ma Fundición pluton, e.g. Streit *et al.* (2015).

The third signature is Neogene zircons (<25 Ma), which are originally sourced from volcanic rocks on the Puna plateau, but can also be reworked from Neogene foreland and intermontane basin deposits. Surprisingly, not all Neogene sediments in the study area contain Neogene zircons. Published spectra from the Pisungo Formation contains them, whereas spectra from the Río Grande and Rio Seco Formations lack them (Decelles *et al.*, 2011; Siks & Horton, 2011), (Fig. 7). In some cases, the precisely known eruptive ages of Neogene volcanic units in the central Andes allow detrital zircons to be linked to specific magmatic centres. A compilation of ages for silicic volcanic units in the study area (Fig. 1) shows a tendency to cluster into a middle Miocene grouping (*ca.* 11–16- Ma) and a Mio-Pliocene cluster (<7 Ma) (Coira *et al.*, 1993; Cladouhos *et al.*, 1994; Petrinovic *et al.*, 1999; Caffe *et al.*, 2002; Prezzi & Gõtze, 2006; Mazzuoli *et al.*, 2008; Kay & Coira, 2009; Salisbury *et al.*, 2011). The closest volcanics to the Río Iruya section are the late Miocene (6–7 Ma) Coránzuli and Panizos complexes, which crop out *ca.* 100 km west of the Río Iruya headwaters (Fig. 1). These units were deposited atop existing mid Miocene volcanic deposits, including the Pozuelos, Pan de Azucar, Chinchilla and Tiomayo/Cara-Cara units, which are *ca.* 12–14.3 Ma in age.

Detrital zircons in the Río Iruya section

The three zircon signatures described above can be used to interpret zircon age spectra from the Mio-Pleistocene Orán Group at Río Iruya (Fig. 8 and Table S2). We identify four different time intervals in which detrital zircon samples are characterized by distinctive zircon spectra: *ca.* 7.6–6.3; *ca.* 6.3–4.0; *ca.* 4.0–2.3 and <2.3 Ma. The first interval (*ca.* 7.6–6.3 Ma) is characterized by two spectra that completely lack Jurassic to Neogene zircons, suggesting the contributing drainage area did not include exposures of the Salta Group, Jurassic-Cretaceous plutons or the Puna volcanics. The second interval from *ca.* 6.3 to 4.0 Ma is marked by the appearance of Jurassic to Neogene zircons, interpreted to signal the addition of a source region containing Salta Group rocks and Neogene ignimbrites. This interval is characterized by the addition of a much larger Neogene zircon population, suggesting a direct connection with Puna volcanics or with young basin sediments containing recycled Neogene volcanic zircons. Also within the third interval, two samples (11c and 12c) show a double-hump Pan African peak and lack Paleozoic-Cretaceous grains, suggesting an important source in late Proterozoic to Ordovician sediments (Puncoviscana, Meson, and Santa Victoria). Because our data only approximately constrain the beginning of the third interval to sometime between 4.3 and 3.5 Ma, we adopt an arbitrary age of 4 Ma. The fourth interval begins
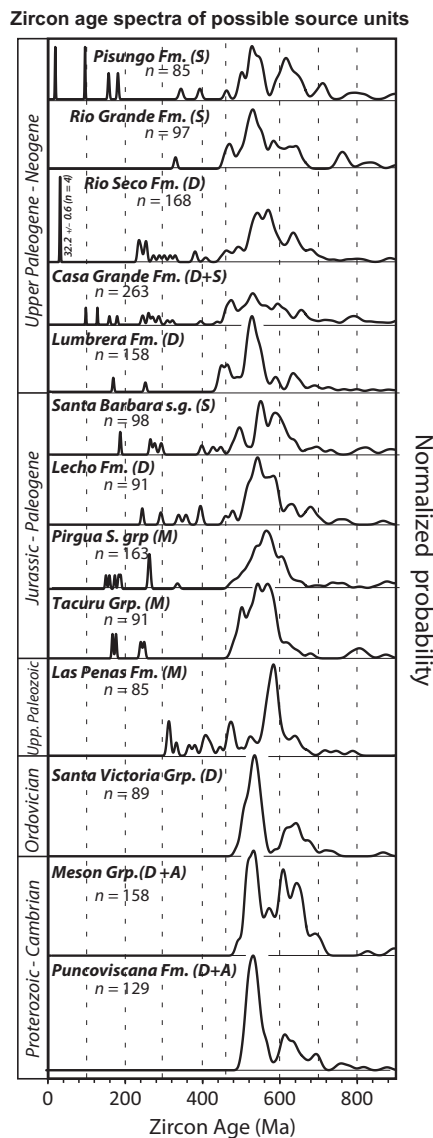

Fig. 7. Detrital zircon spectra of regional sedimentary units compiled from recently published work [Mcbride, 2008 (M), Decelles *et al.*, 2011 (D); Siks & Horton, 2011 (S); Adams *et al.*, 2011 (A)]. Several diagnostic features can be observed, such as the discrete populations constituting the Pan-African 'double hump' between *ca.* 520–720 Ma in the late Proterozoic-Ordovician samples, and the lack of Jurassic-Neogene zircons in the Río Seco and Río Grande formations.
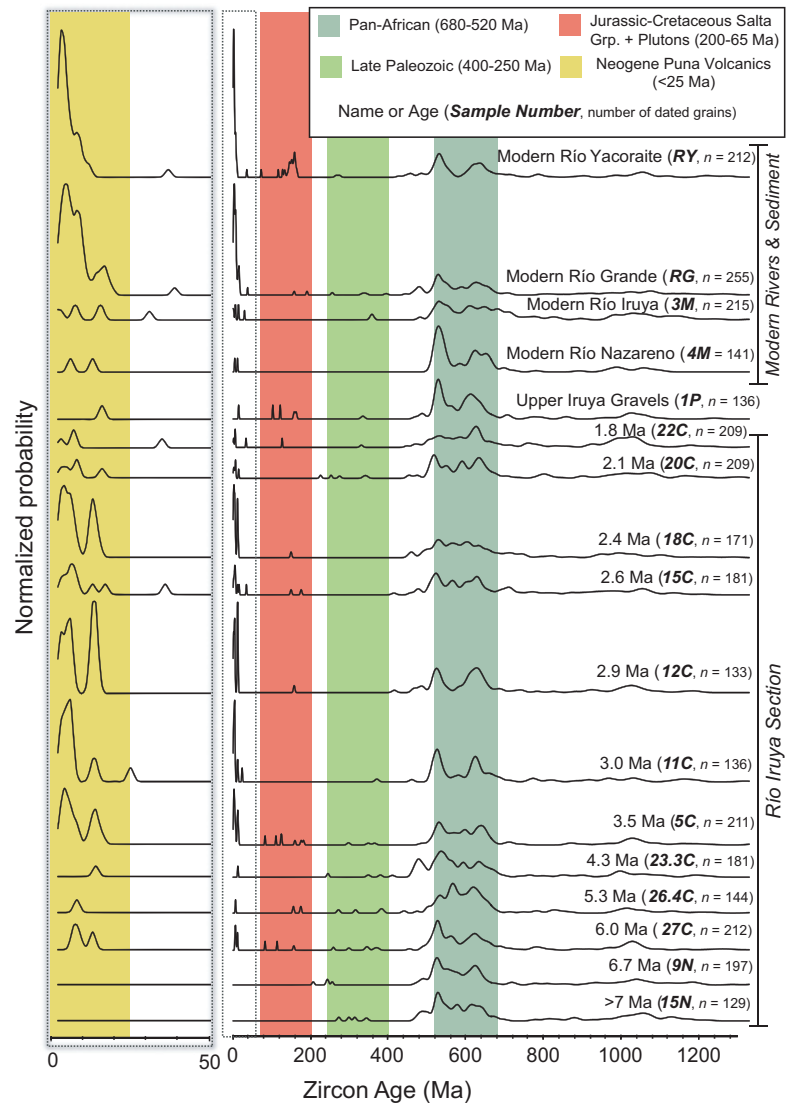
Fig. 8. Detrital zircon spectra from the Orán Group and modern rivers, including the Río Grande and Río Yacoraite from Streit *et al.* (2015). The Orán Group shows three major provenance shifts: 1) the appearance of Jurassic-Neogene zircons at *ca.* 6.3 Ma, 2) the abundance of Neogene zircons from *ca.* 4.0–2.3 Ma, and 3) the decline in Neogene zircons after 2.3 Ma. Samples 11c and 12c show a pronounced 'double hump' Pan-African distribution similar to the modern Río Nazareno and Proterozoic-Paleozoic bedrock units displayed in Fig. 8. Neogene populations from the Río Iruya section show prominent 6–7 and 12–14 Ma peaks, most likely derived from the Panizos caldera and Pozuelos basin.

at *ca.* 2.3 Ma when the population of Neogene zircons decreases dramatically, suggesting a loss of connectivity with Puna volcanics or related sediments.

The visual observations described above are supported by the Kolmogorov–Smirnov (K–S) test (Table S3). Pair-wise comparison of samples in stratigraphic order indicates two statistically significant changes at >99% confidence in the Iruya section, one at *ca.* 4 Ma (*P*-value = 0.007), and one at *ca.* 2.3 Ma (*P*-value = 0.001).

Quartz composition

Quartz compositions from the Orán Group do not record all of the provenance shifts described above, but do lend strong support for an important change in provenance during the 4.0–2.3 Ma interval (Table S4, Fig. 9 and Fig. S2). The shift at *ca.* 4 Ma is marked by a decline in median Fe content (dark blue line; Fig. 9a), and the addition of low Mg and low Ti populations (light blue area;

Fig. 9a). The drop in Ti content is also visible in a plot of Al vs Ti (Fig. S2), which emphasizes an expanded population of extremely low Ti grains after *ca.* 4 Ma. These low Ti grains can only be derived from low-grade metamorphic quartz, most likely the meta-sediments of the Puncoviscana Formation, and perhaps the quartzites of the Meson, and Santa Victoria groups (Götze, 2009). Uniquely low Al, Ti, Fe, Li and K in quartz from sample 12C are remarkably similar to the Puncoviscana Fan (5M), further pointing towards these older metamorphic units as a unique quartz signature.

Quartz data also suggest a more restricted source region during the 4.0–2.3 Ma interval. Clustered principal component scores for samples at 3.5 and 2.9 Ma (5c and 12c) show quartz grains of a restricted compositional range, suggesting quartz was sourced from a restricted drainage area with a narrow range of compositional variability (Fig. 10 and Table S4). In contrast, all other samples show broadly distributed PC scores, suggesting that their
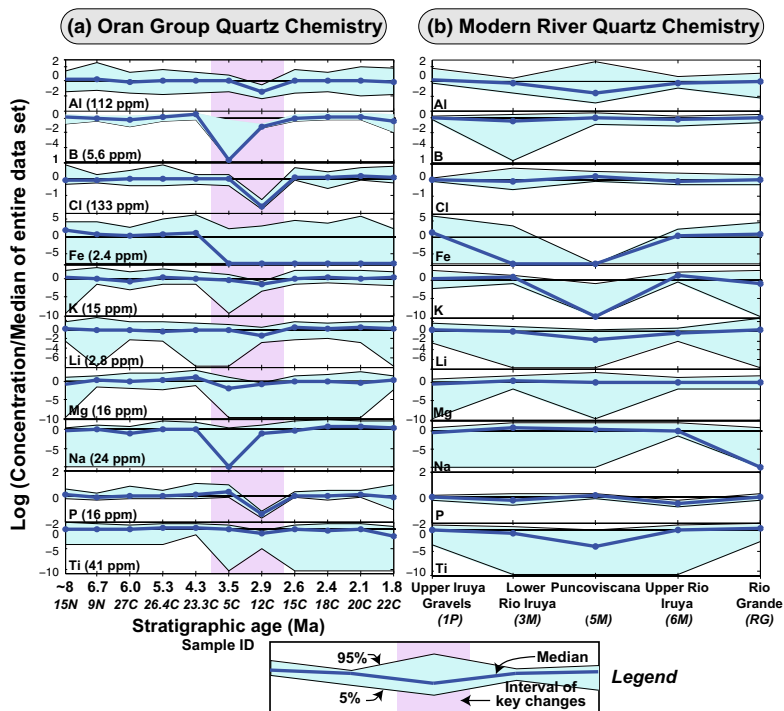
Fig. 9. Modified box and whisker plots summarizing the quartz compositions of (a) Rio Iruya samples, and (b) modern river samples. The plots show three different concentrations on the y-axis.

quartz population is derived from a range of lithologies. Cluster analysis shows the same result; classification pie charts show that quartz from samples 5C and 12C are each dominated by unique populations of quartz (Figs S3 and S4). A restricted source region in the 4.0–2.3 Ma interval agrees with the interpretation drawn from detrital zircon samples 11c and 12c, whose clean 'double hump' signatures suggest a dominant source in the Puncoviscana formation, Meson Group or Santa Victoria Group.

Because we lack quartz data from specific source units, it is difficult to say with certainty whether low trace element metamorphic quartz is derived exclusively from the higher grade Puncoviscana Formation, or whether it may

also be derived from the Meson and Santa Victoria groups. Our own visual observations as well as recent mapping in the Santa Victoria Range confirm numerous ortho-quartzite units in the Meson Group, which appear ideal for generating large amounts of low trace element quartz (Rubiolo, 2003). However, Augustsson *et al.* (2011) conclude that quartzites of the Meson Group are unmetamorphosed and are sandstones held together by silica cement. In their study area south of the Santa Victoria Range they observe the preservation of igneous cathodoluminescence textures in many grains, and conclude that the lower Meson Group is dominated by igneous quartz. If the Meson group is in fact weakly
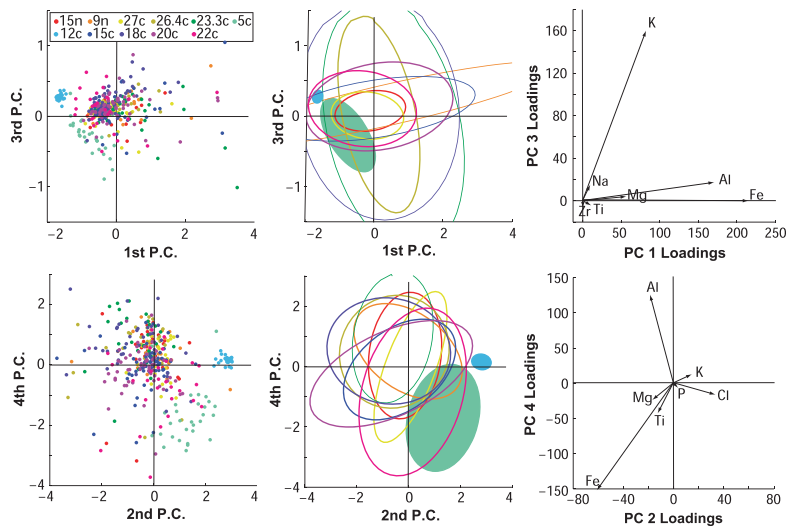

Fig. 10. Principal component scores (left) and 2σ ellipses (centre) for quartz grains and samples. Most samples show a broad scatter suggesting detrital quartz sourced from a range of sources, whereas samples 5c and 12C (filled) show unique clusters suggesting quartz sourced from a restricted region. Plots to the right show the principal component loadings, in which larger vectors correspond to elements that are more important in explaining the observed compositional variability.

metamorphosed (but strongly silicified), the observed metamorphic quartz signal may instead be derived exclusively from the Puncoviscana Formation.

DISCUSSION

Chronology of the Iruya section

Our revised chronology is in agreement with the previously published chronology for the Río Iruya section (Hernández *et al.*, 1996), with several modifications. First, the top of the section has been determined to correlate with the C2n normal period at 1.78–1.95 Ma (Fig. 3), whereas previously the highest normal period had been correlated with the C1r.2n chron between 1.17 and 1.19 Ma (Hernández *et al.*, 1996), shifting the age of the top of the section back *ca.* 0.6 Myr. The previous correlation required a decrease in sedimentation rates to 0.42 km Myr^{-1} after *ca.* 3 Ma (Echavarria *et al.*, 2003; Hernández & Echavarria, 2009). We observe no such decrease in sedimentation rates, seeing instead that accumulation rates remain relatively constant at *ca.* 1 km Myr^{-1} between 2 and 3 Ma.

Implications for regional tectonics

The ca. 7.6–6.3 ma period

Based on the lack of Jurassic-Neogene zircons, the Iruya section does not record erosion of Salta Group or Neogene volcanics during the interval *ca.* 7.6–6.3 Ma. These age populations are also absent from the *ca.* 12–13 Ma Río Grande Formation in the Cianzo Basin (Siks & Horton, 2011), and the *ca.* 16–17 Ma Rio Seco formation at Campamento Vespucio (CV in Fig. 1) (Decelles *et al.*, 2011). We exclude four tightly clustered zircons (32.2 ± 0.6 Ma) from the Rio Seco sample, which are considered as a unique point source below. Similar to Iruya, the Cianzo section acquires the Jurassic-Neogene age populations by the time the Pisungo Formation is deposited, probably in the late Miocene (Fig. 7) (Siks & Horton, 2011). No younger samples are published from the CV site, so it is unclear if or when the Jurassic-Neogene zircon population appears.

Because the Salta Group, Puna volcanics, and Neogene basin sediments are widely exposed near 22° S today (Fig. 1), it is challenging to envision a scenario in which the proto-Iruya, Cianzo and Campamento Vespucio watersheds lacked zircons derived from them. Our preferred explanation is that all of these watersheds were cut off from the Puna Plateau during the mid-late Miocene. This could be achieved if significant relief had existed in the Eastern Cordillera for long enough to completely denude the overlying Salta Group and Oligocene deposits (e.g. the Casa Grande formation). These weakly consolidated units would be stripped off quickly, leaving behind Proterozoic-Devonian meta-sediments, which lack Jurassic-Neogene zircons. In this scenario, the first appearance of Jurassic-Neogene zircons in the Iruya section sometime between 6.7–6.0 Ma could record tectonic reactivation of the Eastern Cordillera, in which additional Salta Group sediments were uplifted and eroded into the foreland, along with more Neogene basin sediments. Renewed tectonism at this time is supported by the onset of deposition of the Maimará Formation at *ca.* 6.5 Ma in the Humahuaca region. This unit was deposited by an unrestricted east-flowing river system, likely in response to westward encroaching tectonism (Pingel *et al.*, 2013).

One problem with the scenario outlined above is the presence of four 32 Ma zircons in the Rio Seco formation, which must have come from a distant magmatic source. The 32 Ma age falls within a well-known temporal gap in magmatism that affected the east-central Andes from about 38–27 Ma (James & Sacks, 1999; Kay & Coira, 2009). As a result, there are very few published sources for 32 Ma zircons in the Central Andes. One possible source is 32 Ma igneous rocks erupted in the Santa Lucia district of the Peruvian Cordillera Occidental about 500 km north west of Iruya near 15°40′ N, 70°35′ W (Sandeman *et al.*, 1995). Another is the magmatic centre at Cerro Ratone about 350 km to the southwest (25.25° S, 66.88° W), which has been dated to 30 ± 3 Ma (Linares & Gonzales, 1990). Thirty-two Ma eruptive centres become more plentiful south of *ca.* 28° S and north of about 15° S in central Peru (Coira *et al.*, 1993; Bissig *et al.*, 2008), but it is unlikely a river system reached this far. Regardless of the exact source of these zircons, they suggest that the paleo-Rio Seco watershed was connected with the Puna interior, or beyond.

The ca. 4.0–2.3 Ma period

The Iruya section seems to record an acceleration of uplift and incision in nearby mountain ranges beginning *ca.* 4 Ma. The first evidence for uplift is a facies change at *ca.* 4 Ma from distal siltstones and sandstones to a proximal gravel-boulder facies in the Iruya section (Fig. 3). This gravel facies continues upwards through the remainder of the section. Secondly, the quartz chemistry and zircon signatures in samples from 3.5 to 2.9 Ma record a restricted source region in meta-sedimentary source rocks of Puncoviscana, Meson and/or Santa Victoria groups – strata that are very widely exposed in the Santa Victoria range immediately to the west (Fig. 2). Thirdly, a significant population of Neogene zircons is added at *ca.* 4 Ma, with particularly prominent age peaks at 6–7 Ma and 12–14.3 Ma zircon peaks. These peaks point to a source region in or around the Pozuelos basin, deriving sediment from the Panizos ignimbrite (*ca.* 6.8 Ma) and earlier 12–14 Ma ignimbrites in the area (Fig. 1). A larger source region would likely have included zircons from older ignimbrites that exist to both the north and south (Fig. 1). Considering this diverse evidence, we propose that the 4-Ma transition records arrival of the proto-Río Iruya, which was incising its current

canyon through the uplifting Santa Victoria and Cincos Picachos ranges (Fig. 2). One idea is that the Rio Iruya once traversed the Santa Victoria range, directly tapping Neogene zircons in the Tres Cruces region. Alternatively, Neogene zircons may have been recycled from Neogene sediments that were stripped as uplift accelerated: a scenario which would not require direct connection to the Puna.

Evidence for accelerated uplift at *ca.* 4 Ma is also observed elsewhere in the region. First, in the Humahuaca region, the transition from the Maimará to Tilcara formations at *ca.* 4.1 Ma is interpreted as a switch from unrestricted foreland conditions to a closed intermontane basin (Pingel *et al.*, 2013). Intermontane conditions are inferred because: (1) Puna volcanic clasts disappear and are replaced by a larger fraction of Puncoviscana and Mesón Group and (2) paleo-currents switch from westerly to southerly. Thus, at the same time that the Humahuaca basin was cut off from the Puna volcanics, the Iruya gained a Puna source. Second, the onset of renewed Pliocene deposition in the nearby Casa Grande basin at *ca.* 4.0 Ma likely records uplift of the Sierra Alta and/or Sierra Aguilar (Streit *et al.*, 2015). The modern Rio Yacoraite contains mostly <7 Ma zircons (Fig. 8), suggesting the Casa Grande basin was disconnected from a source of 12–14 Ma zircons in the Pozuelos region, further evidence for tectonic isolation from the upper Iruya watershed at this time (Fig. 1). Finally, significant reactivation of the Subandean Belt commences about 4.5 Ma, suggesting a change in tectonic regime at this time (Echavarria *et al.*, 2003). Our results suggest that uplift of the Eastern Cordillera was synchronous with out of sequence thrusting in the Subandean Belt.

The <2.3 ma period

The reduction in Neogene zircons after *ca.* 2.3 Ma suggests the Iruya section became disconnected from the Puna volcanics or associated Neogene basin fill. One explanation is that this records defeat of the proto-Iruya river by continued uplift of the Santa Victoria range, effectively severing its headwaters in the Tres Cruces and/or Pozuelos regions (Fig. 1a). One explanation for this defeat could be increasing aridity behind the Eastern Cordillera caused by the growing orographic barrier along its eastern flank. This developing rain shadow would have reduced stream power in the upper Iruya, creating incision rates insufficient to keep pace with uplift of the Santa Victoria range. The 2.3 Ma timing aligns well with increasing isolation of the Casa Grande Basin, which is also interpreted to have been caused by a decrease in sediment supply due to increased aridity (Streit *et al.*, 2015). Alternatively, the loss of these zircons could record the complete stripping of Neogene sediments from atop the growing Santa Victoria Range, or isolation by re-activation of the Pescado thrust at *ca.* 2.3 Ma (Echavarria *et al.*, 2003).

CONCLUSIONS

This study combines dense paleo-magnetostratigraphic sampling with six new U–Pb ages from interbedded ash layers to produce a revised chronology for the Orán Group exposed in the Río Iruya canyon. The new chronology spans 1.94–6.49 Ma, and the resulting age-model provides 95th-percentile age confidence intervals of ±103 kyr on the boundary ages. The revised chronology generally aligns well with the previously published chronology (Hernández *et al.*, 1996), but revises the age of the top of the section back *ca.* 0.6 Myr.

Detrital U–Pb zircon ages and detrital quartz chemistry record three major shifts in sedimentary provenance, which we interpret as tectonically driven drainage reorganization events. From *ca.* 7.6 to 6.3 Ma, a lack of Jurassic-Neogene zircons in the Iruya, Cianzo and Campo Vespucio sections is puzzling. Our preferred explanation is that these sections were isolated from the Puna plateau by existing relief, which had already been stripped of its Jurassic-Neogene cover rocks. The re-appearance of these zircons at *ca.* 6.3 Ma may signal renewed tectonism in the region. At *ca.* 4.0 Ma, the Iruya section records a restricted source region in Proterozoic to Paleozoic metamorphic rocks, along with a new source of Neogene zircons. This combination suggests rapid uplift and incision of the Santa Victoria range by a drainage that may have connected westward to tap the Tres Cruces region. Finally, at *ca.* 2.3 Ma, the Iruya section loses its source of Neogene zircons, perhaps due to disconnection from the Puna Plateau by defeat of the Rio Iruya, or by the complete removal of overlying Neogene sediments from the Santa Victoria Range.

Collectively these observations suggest that much of the modern relief in the Eastern Cordillera at *ca.* 23° may have developed during the latest Miocene and Pliocene. This relief appears to have developed synchronously with shortening in the Subandean Belt, implying simultaneous out-of-sequence thrusting in both the Eastern Cordillera and Subandean Belt.

by the NSF Geomorphology and Land Use Dynamics program through NSF grant EAR-1148233. This award was partially funded by the Vermont EPSCOR program.

CONFLICT OF INTEREST

No conflict of interest declared.

SUPPORTING INFORMATION

Additional Supporting Information may be found in the online version of this article:

Figure S1. Characteristic demagnetization plots for both reversed (a) and normal (b) polarity samples using alternating-field (AF) and thermal demagnetization steps on samples collected from the Río Iruya magnetostratigraphic section. (c) Stereographic equal-area plot of tilt-corrected remanant magnetization directions, with larger circles indicating the $\alpha95$ error around the Fisher mean for both normal and reversed polarities. Additional associated statistics are listed adjacent to the plot. (d) Magnetic moment decay during step-wise AF and thermal demagnetization steps for samples shown in (a) and (b).

Figure S2. Plot of Al vs Ti concentrations for all quartz samples.

Figure S3. Plot of the F-statistic vs the number of clusters defined when applying the K-means clustering algorithm.

Figure S4. Pie charts showing the results of using the K-means clustering algorithm to divide the quartz composition dataset into six arbitrary classes.

Table S1. U-Pb zircon data from air-fall ash deposits.

Table S2. U-Pb zircon data from modern and paleo-detrital samples.

Table S3. Komorogov–Smirnov *P*-values using error in the CDF for detrital zircon samples.

Table S4. Single grain quartz trace element data from detrital samples.

REFERENCES

ACKERSON, M.R., TAILBY, N.D. & WATSON, E.B. (2015) Trace elements in quartz shed light on sediment provenance. *Geochem. Geophys. Geosyst.* doi: 10.1002/2015GC005896.

ADAMS, C.J., MILLER, H., ACENZOLA, F.G., TOSELLI, A.J. & GRIFFIN, W.L. (2011) The pacific Gondwana margin in the late neoproterozoic-early paleozoic: detrital zircon U-Pb ages from metasediments in Northwest Argentina reveal their maximum age, provenance and tectonic setting. *Gondwana Res.*, **19**, 71–83.

ALLMENDINGER, R.W., JORDAN, T.E., KAY, S.M. & ISACKS, B.L. (1997) The evolution of the Altiplano-Puna Plateau of the central Andes. *Annu. Rev. Earth Planet. Sci.*, **25**, 139–174.

AMIDON, W.H., BURBANK, D.W. & GEHRELS, G.E. (2005a) Construction of Detrital mineral populations: insights from mixing of U-Pb zircon ages in Himalayan rivers. *Basin Res.*, **17**, 463–485.

AMIDON, W.H., BURBANK, D.W. & GEHRELS, G.E. (2005b) U-Pb zircon ages as a sediment mixing tracer in the Nepal Himalaya. *Earth Planet. Sci. Lett.*, **235**, 244–260.

AUGUSTSSON, C., RÜSING, T., ADAMS, C.J., CHMIEL, H., KOCABAYOĞLU, M., BÜLD, M., ZIMMERMANN, U., BERNDT, J. & KOOIJMAN, E. (2011) Detrital quartz and zircon combined: the production of mature sand with short transportation paths along the Cambrian West Gondwana margin Northwestern Argentina. *J. Sediment. Res.*, **81**, 284–298.

BISSIG, T., ULLRICH, T.D., TOSDAL, R.M., FRIEDMAN, R. & EBERT, S. (2008) The time-space distribution of eocene to miocene magmatism in the Central Peruvian Polymetallic Province and its metallogenetic implications. *J. S. Am. Earth Sci.*, **26**, 16–35.

BREITER, K., ACKERMAN, L., SVOJTKA, M. & MÜLLER, A. (2013) Behavior of trace elements in quartz from Plutons of different geochemical signature: a case study from the Bohemian Massif, Czech Republic. *Lithos*, **175–176**, 54–67.

BROWN, S.J.A. & FLETCHER, I.R. (1999) Shrimp U-Pb dating of the Preeruption growth history of zircons from the 340 Ka Whakamaru Ignimbrite, New Zealand: evidence for >250 K.Y. Magma Residence Times. *Geology*, **27**, 1035–1038.

CAFFE, P.J., TRUMBULL, R.B., COIRA, B.L. & ROMER, R.L. (2002) Petrogenesis of early Neogene Magmatism in the Northern Puna; implications for magma genesis and crustal processes in the Central Andean Plateau. *J. Petrol.*, **43**, 907–942.

CARRAPA, B., BYWATER-REYES, S., DECELLES, P.G., MORTIMER, E. & GEHRELS, G.E. (2012) Late eocene-pliocene basin evolution in the eastern Cordillera of Northwestern Argentina (25°–26°S): regional implications for Andean Orogenic wedge development. *Basin Res.*, **24**, 249–268.

CARRERA, N. & MUÑOZ, J.A. (2008) Thrusting evolution in the Southern Cordillera oriental (Northern Argentine Andes): constraints from Growth Strata. *Tectonophysics*, **459**, 107–122.

CLADOUHOS, T.T., ALLMENDINGER, R.W., COIRA, B. & FARRAR, E. (1994) Late Cenozoic deformation in the central Andes; fault kinematics from the Northern Puna, Northwestern Argentina and Southwestern Bolivia. *J. S. Am. Earth Sci.*, **7**, 209–228.

COIRA, B., KAY, S.M. & VIRAMONTE, J.M. (1993) Upper cenozoic magmatic evolution of the Argentine Puna; a model for changing subduction geometry. *Int. Geol. Rev.*, **35**, 677–720.

COUTAND, I., CARRAPA, B., DEEKEN, A., SCHMITT, A.K., SOBEL, E.R. & STRECKER, M.R. (2006) Propagation of orographic barriers along an active range front: insights from sandstone petrography and detrital apatite fission-track thermochronology in the intramontane Angastaco Basin, NW Argentina. *Basin Res.*, **18**, 1–26.

DECELLES, P.G. & HORTON, B.K. (2003) Early to middle tertiary foreland basin development and the history of Andean crustal shortening in Bolivia. *Geol. Soc. Am. Bull.*, **115**, 58–77.

DECELLES, P.G., CARRAPA, B., HORTON, B.K. & GEHRELS, G.E. (2011) Cenozoic foreland basin system in the Central Andes of Northwestern Argentina: implications for Andean geodynamics and modes of deformation. *Tectonics*, **30**, TC6013. doi: 10.1029/2011TC002948.

DEEKEN, A., SOBEL, E.R., COUTAND, I., HASCHKE, M., RILLER, U. & STRECKER, M.R. (2006) Development of the Southern Eastern Cordillera, NW Argentina, constrained by Apatite fission track thermochronology: from early cretaceous extension to middle Miocene shortening. *Tectonics*, **TC6003**. doi:10.1029/2005TC001894.

DEL PAPA, C., HONGN, F., POWELL, J., PAYROLA, P., DO CAMPO, M., STRECKER, M.R., PETRINOVIC, I., SCHMITT, A.K. & PEREYRA, R. (2013) Middle Eocene-Oligocene broken-foreland evolution in the Andean Calchaqui Valley, NW Argentina: insights from stratigraphic, structural and provenance studies. *Basin Res.*, **25**, 574–593.

ECHAVARRIA, L., HERNÁNDEZ, R., ALLMENDINGER, R. & REYNOLDS, J. (2003) Subandean thrust and fold belt of Northwestern Argentina: geometry and timing of the Andean evolution. *AAPG Bull.*, **87**, 965–985.

EGE, H., SOBEL, E.R., SCHEUBER, E. & JACOBSHAGEN, V. (2007) Exhumation history of the Southern Altiplano Plateau (Southern Bolivia) constrained by apatite fission-track thermochronology. *Tectonics*, **26**, 24.

ELGER, K., ONCKEN, O. & GLODNY, J. (2005) Plateau-style accumulation of deformation: Southern Altiplano. *Tectonics*, **24**, 1–19.

GÖTZE, J. (2009) Chemistry, textures and physical properties of quartz – geological interpretation and technical application. *Mineral. Mag.*, **73**, 645–671.

GUBBELS, T.L., ISACKS, B.L. & FARRAR, E. (1993) High-level surfaces, plateau uplift, and foreland development, Bolivian central andes. *Geology*, **21**, 695–698.

HAIN, M.P., STRECKER, M.R., BOOKHAGEN, B., ALONSO, R.N., PINGEL, H. & SCHMITT, A.K. (2011) Neogene to quaternary broken foreland formation and sedimentation dynamics in the Andes of Nw Argentina (25°S). *Tectonics*, **30**, TC2006. doi: 10.1029/2010TC002703.

HERNÁNDEZ, R. & BOLL, A. (1986) Interpretacion estructural del area tres cruces. *Bol. Inf. Petroleras*, **AXO III**, 2–14.

HERNÁNDEZ, R. & ECHAVARRIA, L. (2009) Subandean fold and thrust belt of Northwest Argentina: stratigraphy, geometry, and chronology of deformation. *Rev. Asoc. Geol. Argent.*, **65**, 68–80.

HERNÁNDEZ, R., REYNOLDS, J. & DISALVO, A. (1996) Análisis tectosedimentario Y Ubicación Geocronológica Del Grupo Orán En El Río Iruya. *Bol. Inf. Petroleras*, **13**, 80–93.

HERNÁNDEZ, R., GALLI, C.I. & REYNOLDS, J. (1999) Estratigrafía Del Terciario en el Noroeste Argentino. *15° Congreso Geológico Argentino*. G. González Bonorino, R. Omarini & J. Viramonte. Salta, 316–328.

HONGN, F., PAPA, C.D., POWELL, J., PETRINOVIC, I., *et al.* (2007) Middle eocene deformation and sedimentation in the Puna-Eastern Cordillera transition (23°–26°S): control by preexisting heterogeneities on the pattern of initial Andean shortening. *Geology*, **35**, 271.

HORTON, B., PARRA, M., NIE, J., SAYLOR, J., MORA, A., TORRES, V., STOCKLI, D. & STRECKER, M. (2010) Resolving uplift of the Northern Andes using detrital zircon age signatures. *GSA Today*, **20**, 4–10.

INSEL, N., GROVE, M., HASCHKE, M., BARNES, J.B., SCHMITT, A.K. & STRECKER, M.R. (2012) Paleozoic to early cenozoic cooling and exhumation of the basement underlying the Eastern Puna Plateau margin prior to plateau growth. *Tectonics*, **31**, TC6006. doi: 10.1029/2012TC003168.

JACKSON, S.E., PEARSON, N.J., GRIFFIN, W.L. & BELOUSOVA, E.A. (2004) The application of laser ablation-inductively coupled plasma-mass spectrometry to in situ U-Pb zircon geochronology. *Chem. Geol.*, **211**, 47–69.

JAMES, D.E. & SACKS, I.S. (1999) Cenozoic formation of the Central Andes; a geophysical perspective. *Special Publication Soc. Econ. Geol.*, **7**, 1–25.

JONES, C.H. (2002) User-driven integrated software lives: "Paleomag" paleomagnetics analysis on the Macintosh. *Comput. Geosci.*, **28** (10), 1145–1151.

KAY, S.M. & COIRA, B.L. (2009) Shallowing and steepening subduction zones, continental lithospheric loss, Magmatism, and crustal flow under the central Andean Altiplano-Puna plateau. *Geol. Soc. Am. Mem.*, **204**, 229–259.

KIRSCHVINK, J.L. (1980) The least-squares line and plane and the analysis of palaeomagnetic data. *Geophy. J. Int.*, **62**, 699–718.

KIRSCHVINK, J.L., KOPP, R.E., RAUB, T.D., BAUMGARTNER, C.T. & HOLT, J.W. (2008) Rapid, precise, and high-sensitivity acquisition of paleomagnetic and rock-magnetic data: development of a low-noise automatic sample changing system for superconducting rock magnetometers. *Geochem. Geophys. Geosyst.*, **9**, Q05Y01. doi: 10.1029/2007GC001856.

KLEINERT, K. & STRECKER, M.R. (2001) Climate change in response to orographic barrier uplift: paleosol and stable isotope evidence from the late neogene Santa Maria Basin, Northwestern Argentina. *Geol. Soc. Am. Bull.*, **113**, 728–742.

KLEY, J., MÜLLER, J., TAWACKOLI, S., JACOBSHAGEN, V. & MANUTSOGLU, E. (1997) Pre-Andean and Andean-age deformation in the Eastern Cordillera of Southern Bolivia. *J. S. Am. Earth Sci.*, **10**, 1–19.

KYLANDER-CLARK, A.R.C., HACKER, B.R. & COTTLE, J.M. (2013) Laser-ablation split-stream ICP petrochronology. *Chem. Geol.*, **345**, 99–112.

LINARES, E. & GONZALES, R.R. (1990) Catálogo de edades radiométricas de la República Argentina, 1957–1987. *Asoc. Geol. Argent. Publicationes Especiales*, **19B**, 628.

LOURENS, L., HILGEN, F., SHACKLETON, N.J., LASKAR, J. & WILSON, D. (2004) The neogene period. In: *A Geologic Time Scale* (Ed. by F. M. Gradstein, J. G. Ogg & A. G. Smith), Cambridge University Press, Cambridge.

LUDWIG, K.R. (1998) On the treatment of concordant uranium-lead ages. *Geochim. Cosmochim. Acta*, **62**, 665–676.

MAZZUOLI, R., VEZZOLI, L., OMARINI, R., ACOCELLA, V., GIONCADA, A., MATTEINI, M., DINI, A., GUILLOU, H., HAUSER, N., UTTINI, A. & SCAILLET, S. (2008) Miocene magmatism and tectonics of the easternmost sector of the calama-olacapato-El Toro fault system in Central Andes at ~24 degree S: insights into the evolution of the eastern Cordillera. *Geol. Soc. Am. Bull.*, **120**, 1493–1517.

MCBRIDE, S. (2008) Sediment provenance and tectonic significance of the cretaceous Pirgua subgroup, NW Argentina. M.Sc. Thesis, University of Arizona.

MCQUARRIE, N., HORTON, B.K., ZANDT, G., BECK, S. & DECELLES, P.G. (2005) Lithospheric evolution of the Andean fold-thrust belt, Bolivia, and the origin of the central Andean plateau. *Tectonophysics*, **399**, 15–37.

MONECKE, T., KEMPE, U. & GOETZE, J. (2002) Genetic significance of the trace element content in metamorphic and hydrothermal quartz; a reconnaissance study. *Earth Planet. Sci. Lett.*, **202**, 709–724.

MULCH, A., UBA, C.E., STRECKER, M.R., SCHOENBERG, R. & CHAMBERLAIN, C.P. (2010) Late miocene climate variability and surface elevation in the central Andes. *Earth Planet. Sci. Lett.*, **290**, 173–182.

MULLER, A. & KOCH-MUELLER, M. (2009) Hydrogen speciation and trace element contents of igneous, hydrothermal and metamorphic quartz from Norway. *Mineral. Mag.*, **73**, 569–583.

MÜLLER, J.P., KLEY, J. & JACOBSHAGEN, V. (2002) Structure and cenozoic kinematics of the eastern Cordillera, Southern Bolivia (21°S). *Tectonics*, **21**, 1–24.

PETRINOVIC, I.A., MITJAVILA, J., VIRAMONTE, J.G., MARTI, J., BECCHIO, R., ARNOSIO, M. & COLOMBO, F. (1999) Descripcion geoquimica y geocronologica de secuencias volcanicas neogenas de Trasarco, En El Extremo oriental de la Cadena Volcanica transversal del Quevar (Noroeste De Argentina). *Acta Geol. Hisp.*, **34**, 255–272.

PINGEL, H., STRECKER, M.R., ALONSO, R.N. & SCHMITT, A.K. (2013) Neotectonic basin and landscape evolution in the Eastern Cordillera of Nw Argentina, Humahuaca Basin (~24°S). *Basin Res.*, **25**, 554–573.

PREZZI, C. & GÖTZE, H.-J. (2006) 3d modeling of buried intrusives in Pan De Azucar zone (Northern Puna, Argentina) from ground magnetic data. *J. S. Am. Earth Sci.*, **22**, 89–97.

REYNOLDS, J.H., GALLI, C.I., HERNÁNDEZ, R.M., IDLEMAN, B.D., KOTILA, J.M., HILLIARD, R.V. & NAESER, C.W. (2000) Middle miocene tectonic development of the transition zone, Salta Province, Northwest Argentina: magnetic stratigraphy from the Metán subgroup, Sierra De González. *Geol. Soc. Am. Bull.*, **112**, 1736–1751.

REYNOLDS, J.H., HERNÁNDEZ, R.M., GALLI, C.I. & IDLEMAN, B.D. (2001) Magnetostratigraphy of the Quebrada La Porcelana section, Sierra De Ramos, Salta Province, Argentina: age limits for the Neogene Orán group and uplift of the Southern Sierras Subandinas. *J. S. Am. Earth Sci.*, **14**, 681–692.

RUBIOLO, D. (2003) Hoja Geologica 2366-II/2166-IV; La Quiaca. *Programa Nacional de Cartas Geologicas de la Republica Argentina*, Servicio Geologico Minero Argentina, 246.

RUSSO, A. (1975) *Estratigrafía Del Terciario En El Noroeste Argentino*. YPF, Buenos Aires.

SALFITY, J.A. & MARQUILLAS, R.A. (1994) *Tectonic and Sedimentary Evolution of the Cretaceous-Eocene Salta Group Basin, Argentina*. Cretaceous Tectonics of the Andes. J. A. Salfity, Verlag, Teubner.

SALISBURY, M.J., JICHA, B.R., de SILVA, S.L., SINGER, B.S., JIMÉNEZ, N.C. & ORT, M.H. (2011) ^{40}Ar/^{39}Ar chronostratigraphy of Altiplano-Puna volcanic complex ignimbrites reveals the development of a major Magmatic Province. *Geol. Soc. Am. Bull.*, **123**, 821–840.

SANDEMAN, H.A., CLARK, A.H. & FARRAR, E. (1995) An integrated tectono-magmatic model for the evolution of the southern Peruvian Andes (13–20°S) since 55 Ma. *Int. Geol. Rev.*, **37**, 1039–1073.

SCHAERER, U. (1984) The Effect of initial ^{230}Th disequilibrium on young U-Pb ages; the Makalu case, Himalaya. *Earth Planet. Sci. Lett.*, **67**, 191–204.

SCHOENE, B. (2013) U-Th-Pb geochronology. In: *Treatise on Geochemistry* (Ed. by H. D. Holland & K. K. Turekian), 4, pp. 341–378. Elsevier, Oxford.

SIKS, B.C. & HORTON, B.K. (2011) Growth and fragmentation of the Andean foreland basin during eastward advance of fold-thrust deformation, Puna plateau and Eastern Cordillera, Northern Argentina. *Tectonics*, **30**, TC6017. doi: 10.1029/2011TC00294.

SLÁMA, J., KOŠLER, J., CONDON, D.J., CROWLEY, J.L., GERDES, A., HANCHAR, J.M., HORSTWOOD, M.S.A., MORRIS, G.A., NASDALA, L., NORBERG, N., SCHALTEGGER, U., SCHOENE, B., TUBRETT, M.N. & WHITEHOUSE, M.J. (2008) Plešovice zircon - a new natural reference material for U-Pb and Hf isotopic microanalysis. *Chem. Geol.*, **249**, 1–35.

STACEY, J.S. & KRAMERS, J.D. (1975) Approximation of terrestrial lead isotope evolution by a 2-stage model. *Earth Planet. Sci. Lett.*, **2**, 207–221.

STARCK, D., ANZOTEGUI, L.M., GONZALEZ-BONORINO, G., KRAEMAR, P. & RE, G. (2001) The late miocene climatic change; persistence of a climatic signal through the orogenic stratigraphic record in Northwestern Argentina. *J. S. Am. Earth Sci.*, **14**, 763–774.

STRECKER, M.R., ALONSO, R.N., BOOKHAGEN, B., CARRAPA, B., HILLEY, G.E., SOBEL, E.R. & TRAUTH, M.H. (2007) Tectonics and climate of the southern central Andes. *Annu. Rev. Earth Planet. Sci.*, **35**, 747–787.

STREIT, R.L., BURBANK, D.W., STRECKER, M.R., ALONSO, R.N., COTTLE, J.M. & KYLANDER-CLARK, AR. (2015) Controls on intermontane basin filling, isolation, and incision on the margin of the Puna Plateau, NW Argentina (~23°S). *Basin Res.*, In Press.

TAUXE, L. & WATSON, G.S. (1994) The fold test: an Eigen analysis approach. *Earth Planet. Sci. Lett.*, **122**, 331–341.

UBA, C.E., KLEY, J., STRECKER, M.R. & SCHMITT, A.K. (2009) Unsteady evolution of the Bolivian Subandean thrust belt: the role of enhanced erosion and Clastic wedge Progradation. *Earth Planet. Sci. Lett.*, **281**, 134–146.

VIRAMONTE, J.G., KAY, S.M., BECCHIO, R., ESCAYOLA, M. & NOVITSKI, I. (1999) Cretaceous rift related Magmatism in central-western South America. *J. S. Am. Earth Sci.*, **12**, 109–121.

WARK, D.A. & WATSON, E.B. (2006) Titaniq: a titanium-in-quartz Geothermometer. *Contrib. Miner. Petrol.*, **152**, 743–754.

WIEDENBECK, M. (1995) Three natural zircon standards for U-Th-Pb, Lu-Hf, trace element and Ree analyses. *Geostandards Newslett.*, **19**, 1–23.

WOODHEAD, J.D., HELLSTROM, J., HERGT, J.M., GREIG, A. & MAAS, R. (2007) Isotopic and elemental imaging of geological materials by laser ablation inductively coupled plasma-mass spectrometry. *Geostand. Geoanal. Res.*, **31**, 331–343.